

Influence of Reflected Arc Light on Vision Sensors for Automatic GTAW Systems

A model was developed to predict arc noise for various configurations of sensors, base metals, and welding arcs

BY J.-Y. YU, J.-I. KIM, AND S.-J. NA

ABSTRACT. Because of the difficulty in applying arc sensors to the welding of thin corrugated plates, vision sensors that provide three-dimensional geometry information by optical triangulation have been widely used for robot guidance in automatic welding of plates.

The reliability of vision sensors, however, is influenced considerably by arc light reflected from the base metal surface in spite of blocking the direct arc light with a light isolator. A reflectance model of a welding arc was developed to estimate arc noise for various configurations of sensors, base metals, and welding arcs in three-dimensional space by assuming the welding arc as a point and extended light source.

Various experiments were conducted to determine the bidirectional reflectance distribution function (BRDF) parameters of the model, and to verify the validity of the proposed model. Two proposed models, the point source model and the extended source model, were compared with the gray level of the reflected arc caught by a CCD camera. The experimental data of the gray level of the reflected arc generally agreed well with calculated results obtained by the two models, while the model with a point light source resulted in a greater discrepancy for short distances between the welding arc and reflecting surface of the base metal.

The proposed models and experimental results can be effectively used for optimal design of the configuration and the moving path of vision sensors according to base metal shape, which improves the measuring efficiency of vision sensors (Refs. 1, 2) and reduces the effect of arc

noise on them (Ref. 3), thus enhancing the performance of the vision sensor in automatic joint tracking of the arc welding process.

Introduction

Vision sensors are one of the most powerful forms of noncontact sensory feedback for monitoring and control of manufacturing processes such as welding. Machine vision applications in welding have included off-line determination of the locations of the workpieces to be welded (typically referred to as part finding); the in-process correction of robot paths to compensate for fixturing inaccuracies, part tolerances, or weld distortions during welding (joint tracking); the real-time sensing of weld joints, pool shape, and geometry for control of the welding process; and automated inspection of weld joints and bead surface shapes. However, welding poses particularly challenging problems to conventional optical sensing techniques. One of the major problems is the presence of the welding arc, which is not limited to a single spectral region (Refs. 4–8) and is thus difficult to filter optically. A novel vision sensing technique has been developed and is used to overcome the extreme variations in scene brightness created by the welding arc (Refs. 9–15). However, resolution and

field of view were the primary considerations in the design of vision sensors, while sensor reliability was only rarely investigated. Lenef et al. (Ref. 16) measured the arc spectrum to find the wavelength range of the diode laser, which would minimize arc effect. In their experiments, the base metal shape was neglected and the diffuse reflection was assumed for the base metal surface. Nakata et al. (Ref. 17) studied the optimal configuration of optical components by varying the position and resolution of the camera and light source, camera exposure, and other factors. The results, however, were limited in practical application because the arc light was neglected and there was a lack of theoretical understanding in analyzing the experimental results. Various reflectance models have been used in the area of machine vision. Broadly speaking, these models can be classified into two categories: diffuse reflectance models and specular reflectance models. Until now, many applications have proven that the Lambertian model and the Torrance-Sparrow model adequately describe general diffuse and specular lobes in the vision research community (Refs. 18–20).

Because existing research (Refs. 21, 22) mostly deals with the arc light as a point source carried out in the same plane as the incident beam, those results should be applied only to the situation where vision sensors and the arc generated under the welding gun are positioned on the same plane. Wang has modeled the arc as a cylindrical shape in studies of arc light generated from an arc plasma (Ref. 23). Such a model should closely approximate the actual shape in order to precisely represent the intensity of the arc light in the short distance between the considered point on the base metal and the welding arc. It is important the arc shape is modeled sufficiently (Ref. 24); therefore, the shape of the arc light can be simplified as a half-hemisphere, which represents the

KEY WORDS

Vision Sensor
Joint Tracking
Light Reflectance
Arc Noise
Point Source
Extended Source

J.-Y. YU and J.-I. KIM are with Mechanical Engineering Division, Advanced Reactor Development, Korea Atomic Energy Research Institute, Korea. S.-J. NA is with Department of Mechanical Engineering, Korea Advanced Institute of Science and Technology, Korea.

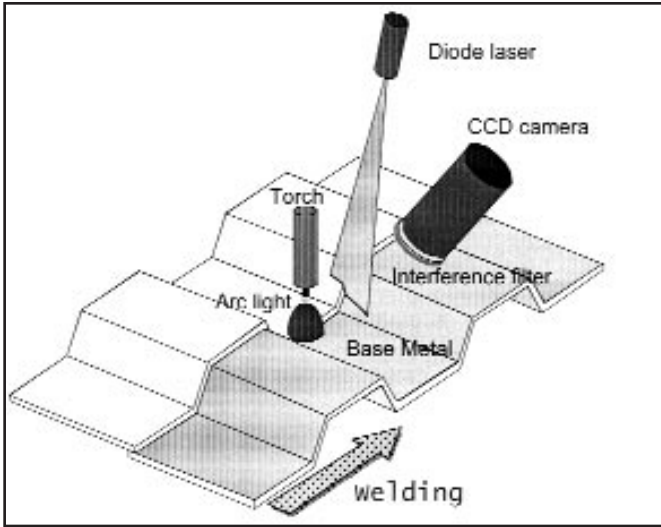


Fig. 1 — Schematic of an automatic welding system with vision sensor.

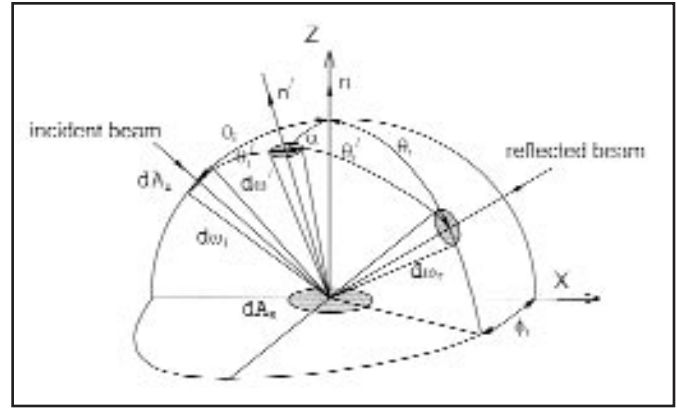


Fig. 2 — Coordinate system for defining BRDF.

arc shape in automatic welding (Ref. 25).

In order to improve the reliability of vision sensors in arc welding, the effect of arc light was investigated as to the geometrical configuration of the vision sensor and the welding arc in a three-dimensional space where various reflection properties of the base metal surface are considered. Base metal reflection was modeled in a three-dimensional (3-D) domain, and the intensity of the arc image was formulated by assuming the arc light as an extended light source.

Theoretical Formulation

Figure 1 shows the typical configuration of an automatic welding system with a visual joint tracking sensor, such as corrugated sheets used for inside walls of LNG tanks or shipping containers. The laser beam is reflected from the base metal surface in front of the welding arc, and the image pattern captured by the CCD camera is used to determine the shape of the weld joint. An interference filter in the camera allows only light with a wavelength range near the laser beam to pass through. At the same time, the arc light is also reflected from the base metal surface and captured by the CCD camera through the interference filter. The intensity of reflected arc from the base metal changes continuously, because the configuration of the vision sensor and torch must be varied according to the motion of the manipulator for joint tracking. In this study, only the arc noise reflected from the sensing area of the base metal surface covered by the CCD camera was considered in formulating the magnitude of the arc light in accordance with the three-dimensional configuration of the arc, base metal, and camera. The preview distance of the

joint tracking vision sensor must also be considered because this parameter significantly contributes to the intensity variation of arc noise.

Reflectance Model of Surface

The local coordinates system was adopted to represent general reflectance characteristics. The angular distribution of the reflected radiant flux is conventionally expressed in terms of the bidirectional reflectance. Consider the geometry shown in Fig. 2. This coordinate system was used to derive the Torrance-Sparrow model. More detailed derivation is given in Refs. 19 and 20. The surface area dA_s is located at the origin of the coordinate frame, and its normal vector point in the direction of z axis. The surface is illuminated by a beam of light that lies in the x - z plane and is incident on the surface at the angle θ_i . The direction (θ_r, ϕ_r) determines the surface radiance for the viewing direction of the vision sensor, which is the direction of interest. Only those planar microfacets whose normal vectors lie within the solid angle $d\omega'$ are capable of specularly reflecting light into the infinitesimal solid angle $d\omega_r$.

The BRDF f_r is defined for the general expression of reflectance as follows:

$$f_r(\theta_i, \phi_i; \theta_r, \phi_r) = \frac{dL_r(\theta_i, \phi_i; \theta_r, \phi_r)}{dE_i(\theta_i, \phi_i)} \quad (1)$$

where $dE_i(\theta_i, \phi_i)$ is the irradiance in the direction of (θ_i, ϕ_i) and $dL_r(\theta_i, \phi_i; \theta_r, \phi_r)$ is the reflected radiance in the direction of (θ_r, ϕ_r) caused by $dE_i(\theta_i, \phi_i)$. The radiance of a Lambertian surface is proportional to its irradiance.

The surface irradiance dE_i produced by incident radiance dL_i is determined by dividing the radiant flux by surface area dA_s and expressed as follows:

$$dE_i(\theta_i, \phi_i) = L_i(\theta_i, \phi_i) \cos\theta_i d\omega_i \quad (2)$$

where $d\omega_i = \sin\theta_i d\theta_i d\phi_i$ is the infinitesimal solid angle. By integrating Equation 2 in all directions on the hemispherical surface, E_i is obtained as follows:

$$E_i(\theta_i, \phi_i) = \int_w L_i(\theta_i, \phi_i) \cos\theta_i d\omega_i \quad (3)$$

$L_r(\theta_r, \phi_r)$ is proportional to its irradiance $E_i(\theta_i, \phi_i)$. Thus, in a similar way, it can be obtained from Equations 1 and 3 with the following:

$$L_r(\theta_r, \phi_r) = \int_w f_r E_i(\theta_i, \phi_i) \cos\theta_i d\omega_i \quad (4)$$

It was considered that the BRDF f_r was composed of fractions of the diffused reflection f_{rd} and specular reflection f_{rs} . The polar plot of the three reflection components (diffuse lobe, specular lobe, and specular spike) is shown in Fig. 3.

$$f_r = f_{rd} + f_{rs} \quad (5)$$

The BRDF f_{rd} has a constant value κ_{diff} which represents the level of diffused reflection. The BRDF f_{rs} is dependent on the surface of the workpiece, since different models are available according to the ratio between the *rms* value of the surface roughness R_q and light wavelength λ (Ref. 20). In the case of $R_q/\lambda \ll 1$, the specular reflection has the same property as on the mirror

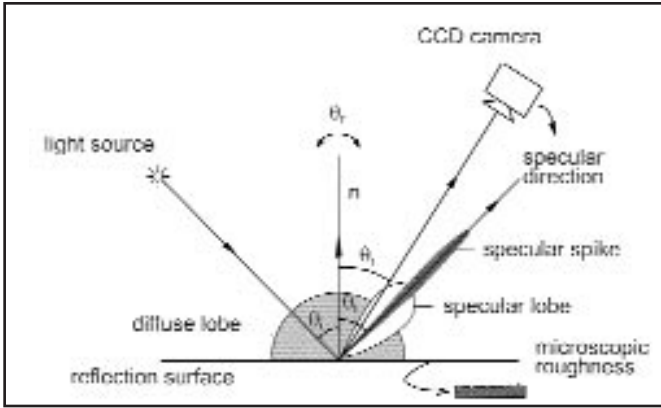


Fig. 3 — Schematic of three reflection components.

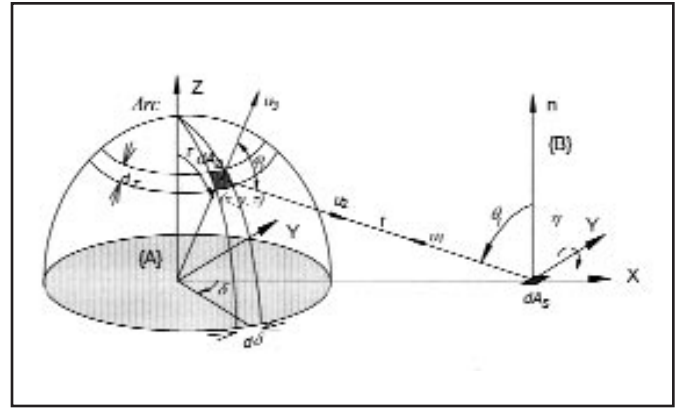


Fig. 4 — Coordinate system of arc shape and reflection point.

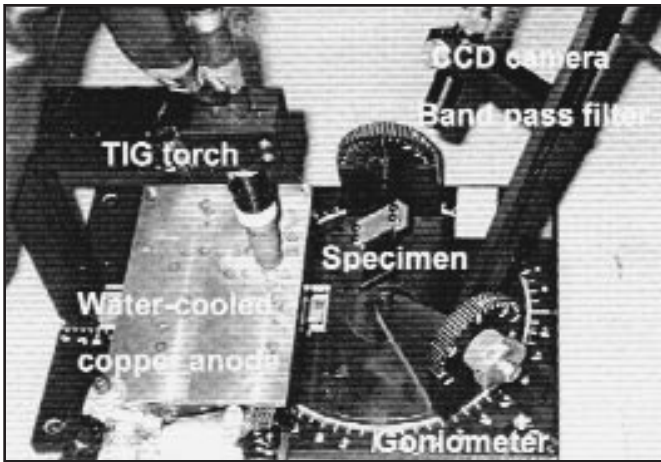


Fig. 5 — Apparatus for experiments of arc noise.

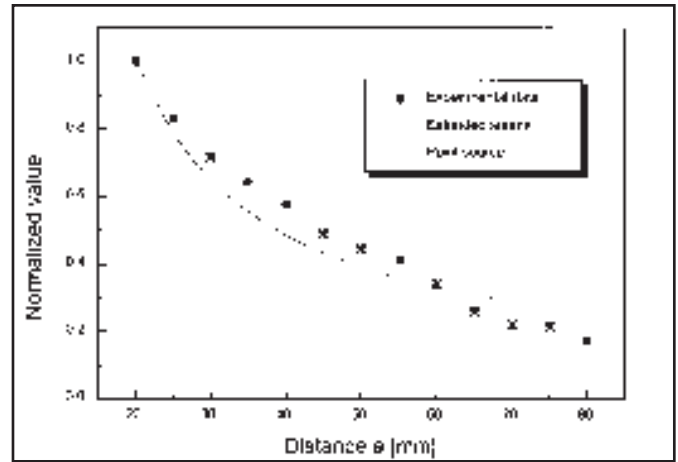


Fig. 6 — Intensity of gas tungsten arc reflected from mild steel with varying distance a ($\theta_i = 70$ deg, $\theta_r = 20$ deg, $\phi_r = 0$ deg).

and is modeled in 3-D as follows:

$$f_{rs} = \delta(\theta_r - \theta_i)\delta(\phi_r - \phi_i - \pi) \quad (6)$$

where $\delta(\theta_r - \theta_i)\delta(\phi_r - \phi_i)$ is a function that satisfies the following:

$$\delta(\theta_r - \theta_i)\delta(\phi_r - \phi_i) = 1$$

for $\theta_r = \theta_i$ and $\phi_r - \phi_i = \pi$

$$\delta(\theta_r - \theta_i)\delta(\phi_r - \phi_i) = 0$$

for $\theta_r \neq \theta_i$ or $\phi_r - \phi_i \neq \pi$

In the case of $R_q/\lambda \gg 1.5$, Torrance et al. established a model based on the assumption the rough surface was composed of specular elements arranged arbitrarily, and that Fresnel reflectance of a material has only a negligible effect on BRDF (Ref. 26). Ignoring the variation of the Fresnel reflectance in accordance to the angle change, the Torrance-Sparrow model can be expressed as follows:

$$f_{rs} = \kappa_{spec} \left[\frac{G(\theta_i, \phi_i, \theta_r, \phi_r)}{\cos \theta_r} \right] \exp(-c^2 \alpha^2) \quad (7)$$

where κ_{spec} is the fraction of specular reflection and c is the statistical distribution of the direction of specular elements. Using spherical trigonometry, the local angle of incidence θ_i and slope α of the reflecting facets can be determined from angle θ_p , θ_r , and ϕ_r in Fig. 2. $G(\theta_p, \theta_r, \phi_p, \phi_r)$ was termed the geometrical attenuation factor, which included consideration of the effect of neighboring specular elements. A detailed derivation is given in Refs. 19, 20.

In the case of $R_q/\lambda \approx 1$, formulation of the specular reflection is quite complex and can be performed only by applying the physical model using wave optics. However, it has been shown that the Torrance-Sparrow model can very accurately predict specular reflection in this case, if no peak values occur. Furthermore, this case is only rarely encountered in applications of vision-aided welding systems, and thus was not formulated in the study.

Arc Noise Model

The welding arc is an electrically conductive gas called plasma, which is considered to be the fourth and most complex

state of matter. The arc-column plasma is produced by the electrical breakdown of normally nonconducting gases between the electrode and the workpiece. Electrical breakdown of the gas occurs through ionization, the process of stripping electrons from atoms. The energy spectrum radiated from the welding arc is composed of characteristic spectral lines of the plasma elements and ions and the black body emission (Refs. 6, 17, 21). The position and intensity of the characteristic spectral lines are known to be strongly influenced by welding conditions, base metal, and shielding gas, while the black body emission of the arc spectral radiance $L_\lambda(\lambda)$ can be expressed by Planck's Law.

In general, configuration of the arc and the point measured by a vision sensor in joint tracking is shown in Fig. 3. If the effective area (A_{eff}) of the arc, which is defined as the part of the arc viewed from the center of the area of interest on the base metal, is relatively large compared to the square of the distance between the arc and base metal (a^2), the arc light must be assumed to be not a point light source, but an extended light source. The model of the arc shape should be close to its actual

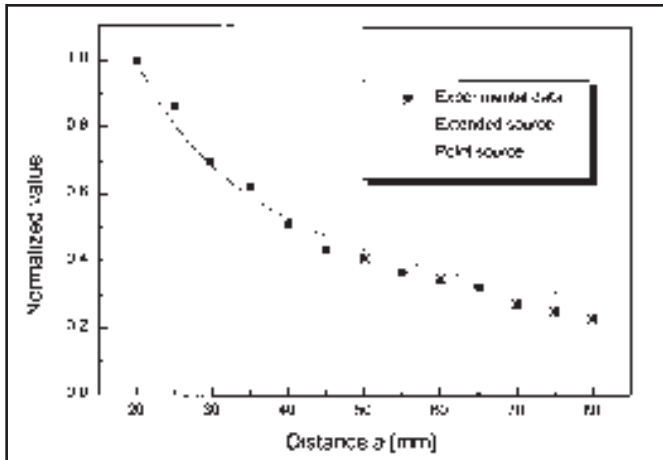


Fig. 7 — Intensity of gas tungsten arc reflected from Zn-coated container panel with varying distance a ($\theta_i = 30$ deg, $\theta_r = 60$ deg, $\phi_r = 0$ deg).

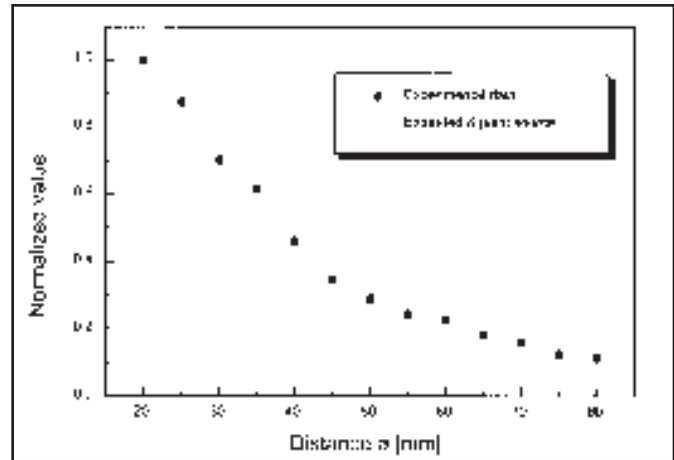


Fig. 8 — Intensity of gas tungsten arc reflected from stainless steel with varying distance a ($\theta_i = 50$ deg, $\theta_r = 50$ deg, $\phi_r = 0$ deg).

shape because the arc shape affects the geometry in short distances between the point of consideration on the base metal and the welding arc. Thus, the shape of the arc is assumed to be half-spherical similar to the real arc.

Total irradiance on dA_s produced by the arc was obtained by integrating the effective area of the arc.

$$E_i = I_\lambda(\lambda) \int_{Arc} \frac{\cos\varphi_i \cos\theta_i}{r^2} dA_a \quad (8)$$

where $I_\lambda(\lambda)$ means the spectral radiant intensity of the arc ($W/(sr \text{ \AA})$), which is assumed to be constant in this research because of a concern in formulation to define the influence and the geometrical relationship of the arc to the position of the vision sensor. Discussion continues about the problem of the optical thinness and thickness in the arc radiation, but this study dealt with the relative amount of radiation from the arc to the CCD camera, resulting from the complicated geometrical and reflective mechanism of the arc plasma.

Extended Light Source Model of the Arc

The effective area of arc is assumed to be a half-hemisphere, so Equation 8 can be expressed as follows:

$$E_i = I_\lambda(\lambda) \int_{-\pi/2}^{\pi/2} \int_0^{\pi/2} \frac{\cos\varphi_i \cos\theta_i}{r^2} dA_a \quad (9)$$

The area dA_a is normal to the (τ, δ) direction, namely, vector u_3 . It may be represented as $dA_a = a^2 \sin\tau d\tau d\delta$ for a spherical surface. Parameters r^2 , $\cos\theta_i$, and $\cos\varphi_i$ vary according to points on the arc. Therefore, r^2 can be expressed as the two vari-

ables τ and δ . The distance between the arc and base metal is a and the radius of the welding arc is R .

$$r^2 = R^2 + a^2 - 2aR\sin\tau\cos\delta \quad (10)$$

The polar angle of the incident beam can be determined by using surface normal vector n and direction vector u_i from the following:

$$\cos\theta_i = \frac{n \cdot \bar{u}_i}{|n| |\bar{u}_i|} \quad (11)$$

where η is the slope of the base metal at the corrugation; symbol \cdot represents the inner product of vectors; and direction vector \bar{u}_i lies on the line from the infinitesimal area dA_s on the base metal to an arbitrary point on the arc.

φ_i is the angle between the normal vector \bar{u}_3 of the infinitesimal area of arc and its incident line. Therefore, $\cos\varphi_i$ can be obtained in the same manner as Equation 11:

$$\cos\varphi_i = \frac{\bar{u}_2 \cdot \bar{u}_3}{|\bar{u}_2| |\bar{u}_3|} \quad (12)$$

If the coordinate frame of the base metal {B} is sloped as η , the azimuthal angle of the infinitesimal area of the arc about the coordinate frame of the sloped base metal is as follows:

$$\tan\phi_i = \frac{y}{(x-R)\cot\eta + z\sin\eta} \quad (13)$$

The radiance of the reflected arc from the base metal $L_r(\lambda)$ can be modeled by assuming the arc as an extended source as follows:

$$L_r(\lambda) = I_\lambda(\lambda) \int_{-\pi/2}^{\pi/2} \int_0^{\pi/2} \frac{\cos\varphi_i \cos\theta_i}{r^2} a^2 \sin\tau d\tau d\delta \quad (14)$$

Point Light Source Model of Arc

If the arc is assumed to be a point light source, the general equation above can be simplified. The angle between the surface normal vector and the tangential plane of effective area are constant. If the effective lighting area of the arc concerns only the radiation, effective area can be expressed as follows:

$$dA_{eff} = \cos\varphi_i dA_a \quad (15)$$

If the effective area on the arc is negligibly smaller than the square of the distance between the arc and concerned area dA_s on the base metal, namely $A_{eff}/a^2 \ll 1$, $\cos\theta_i/r^2$ can be assumed to be constant in the period of integration. Irradiance E_i can be modeled by assuming the arc as a point light source as follows:

$$E_i = A_{eff} I_\lambda(\lambda) \frac{\cos\theta_{i0}}{a^2} \quad (16)$$

The radiance of the reflected arc from the base metal $L_r(\lambda)$ can be modeled by assuming the arc as a point source as follows:

$$L_r(\lambda) = f_r(\theta_i, \phi_i; \theta_r, \phi_r) A_{eff} I(\lambda) \frac{\cos\theta_{i0}}{a^2} \quad (17)$$

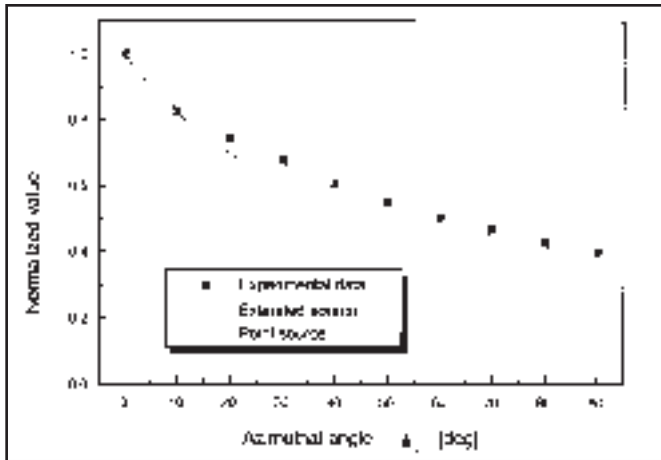


Fig. 9 — Intensity of gas tungsten arc reflected from mild steel with varying azimuthal angle ϕ_r ($a = 30$ mm, $\theta_i = 55$ deg, $\theta_r = 45$ deg).

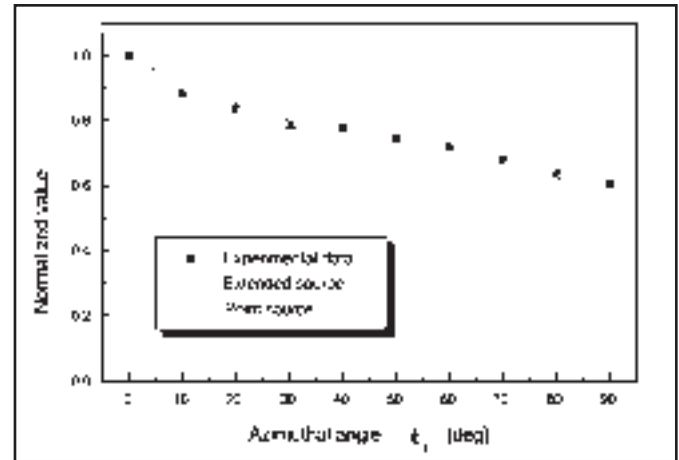


Fig. 10 — Intensity of gas tungsten arc reflected from Zn-coated container panel with varying azimuthal angle ϕ_r ($a = 30$ mm, $\theta_i = 55$ deg, $\theta_r = 45$ deg).

Image Forming Model

Arc light reflected from the base metal surface is filtered through the interference filter, condensed through the lens, and finally captured by the CCD camera to produce an image. The relationship between the spectral radiance $L_r(\lambda)$ caused by the reflection on a surface point and the corresponding irradiance E on the image plane is modeled by considering the pass band of the interference filter. Light power is concentrated in the image (if losses in the lens are ignored). Since no light from other areas reaches this image patch, the irradiance of the patch on the image plane corresponding to the patch on the object surface can be expressed as follows:

$$E = L \frac{\pi}{4} \left(\frac{d}{f} \right)^2 \cos^4 \zeta \quad (18)$$

The above equation reveals that E is in a direct proportion to the radiance of the arc light through the lens. This is the fundamental relationship used to recover information about objects from their images. The factor of proportionality in the formula above contains the inverse square of the effective f -number of the CCD camera, f/d . It also includes a term that falls off with the cosine to the fourth power of the angle made by the ray from the image point to the center of the lens with the optical axis. In this study, this falloff in sensitivity is not important when the image covers only a narrow angle, and the sensing area of the pixels of the vision sensor is very small compared to the distance between the lens and measuring point.

Generally, vision sensors used in automatic welding systems have attached opti-

cal interference filters in order to reduce the influence of arc light in welding. The arc light reflected from the surface is filtered through the interference filter. The irradiance of the image due to reflected arc light from the base metal can be represented as follows, when the optical interference filter is attached to the front of the lens:

$$E(\lambda_c) = \left[\frac{\pi}{4} \left(\frac{d}{f} \right)^2 \cos^4 \zeta \right] \int_0^\infty L_r(\lambda) F_G(\lambda - \lambda_c) d\lambda \quad (19)$$

where λ_c is the center wavelength of the optical interference filter. The value $F_G(\lambda)$ is the spectral response of the optical interference filter, and can be expressed in the Gaussian distribution. The image sensor converts irradiance E into gray level G_I , which is expressed as follows.

$$G_I = pE^\gamma \quad (20)$$

where the p is the proportional constant and γ is the characteristic that is normally 1 for measurements, resulting in a proportional relationship between G_I and E .

Simulation and Experiment

Experiments for BRDF Parameters

In order to determine the BRDF from the reflectance model of arc light for applicable materials used in height-varying weldments, the three BRDF parameters K_{diff} , K_{spec} , and c^2 must be obtained

through experiments. A diode laser with a wavelength λ of 690 nm, which has been widely used in active vision sensors, was employed to determine these constants, because it can be easily suited to satisfy conditions of the reflectance model of the arc light passing through the optical interference filter of the vision sensor. The diode laser supplied the parallel light and the image it projects on the specimen is seen as a point, and the image is captured by a CCD camera with a γ characteristic value of 0.45 in order to expand the dynamic response range of a CCD camera about the high spectral intensity of the light source. A bandpass filter having the same wavelength as the laser and the FWHM of 10 nm was placed in front of the CCD camera to consider the actual configuration of the practical vision sensor used in automatic welding.

The specimens were prepared from hot-rolled mild steel, Zn-coated container panel, and 304 stainless steel, and their surface roughness was measured by atomic force measurement (AFM). The ratios R_q/λ of mild steel and Zn-coated container panel were larger than 1.5; therefore, the surface of these specimens had both diffuse and specular characteristics, which could be applied to Lambert and Torrance's BRDF model. However, the ratio R_q/λ of SUS304 stainless steel was less than 1; therefore, obtaining the BRDF parameter for this specimen was not possible.

The angle of reflection was varied in a wide range, while the angle of incidence was fixed at values between 10 deg and 80 deg. These gray level values obtained directly from the CCD camera were then normalized with regard to maximum gray level. As expected from the Torrance-Sparrow model, these results showed

Table 1 — Results of Nonlinear Regression for Mild Steel Plate and Zn-Coated Container Panel Using Gauss-Newton Method

Parameters	K_{diff}	K_{spec}	C^2	K_{spec}/K_{diff}
Mild steel plate	0.021	0.326	112	15.52
Zn-coated container panel	0.495	0.153	8.331	0.309

characteristics of a diffuse lobe, a specular lobe, and a specular spike. The characteristics of a specular lobe and a specular spike were especially dominant in the mild steel specimen, the other side, the characteristic of a diffuse lobe was mainly an effect of surface reflectance in the container panel specimen. These normalized data were used in the nonlinear regression with the Newton-Gaussian method to obtain three BRDF parameters of Equations 5 and 7. The resultant κ_{diff} , κ_{spec} and c^2 values are shown in Table 1.

Experiments for Arc Noise Models

A photograph of the experimental apparatus is shown in Fig. 5, showing components such as the gas tungsten arc welding torch, water-cooled copper anode, CCD camera and optical band pass filter. The center wavelength of the optical band-pass filter is 690 nm with a bandwidth of 10 nm in front of CCD camera. In order to avoid the direct influence of arc light to CCD camera without reflectance of specimen, during the experiment the isolator was installed between the arc plasma and the CCD camera except the pass of arc light from arc plasma to specimen. And the concerned area in FOV (field of view) of CCD camera is 4 mm² (2

x 2 mm) at the center of the specimen. This experimental apparatus had devices with goniometers that could change the slope of the specimen, the azimuthal angle, the reflected angle, and the distance between the arc and reflected area. The experiments were performed with gas tungsten arc welding (GTAW) at 100 A; tungsten tip-to-workpiece distance was 5 mm. In order to generate a constant and stable arc, a water-cooled copper anode, which could not be melted during welding, was used in the experiments. The magnitude of the gray level of reflected arc light from each specimen was obtained by averaging 20 values measured every 0.2 s. To investigate the validity of the assumptions of considering the arc light as an extended light source and a point light source, the reflected arc light was first measured for various a values at fixed angles of incidence and reflection, then for various azimuthal angles of reflection and reflected angles under the fixed relatively short a . In two cases, the fixed distance a between the arc and reflection area was determined to be 30 mm, because too large a values would greatly decrease the assumption of an extended light source, which would be proved by the experiments by varying the distance a for the incident and reflected fixed angles.

Results and Discussion

Figures 6, 7, and 8 show the gray level of the arc in GTAW reflected from a hot-rolled mild steel plate, Zn-coated container panel, and SUS304 stainless steel with respect to the distance between the arc and reflection area. The experimental data were determined by normalizing the gray levels of the CCD camera with regard to the value at minimum R after compensating them with the gamma characteristic

γ of the CCD camera. That is, $(\text{measured gray level})^{1/\gamma}$ was divided by $(\text{maximum gray level})^{1/\gamma}$ to take into account the spectral response of the CCD camera because its gamma characteristic γ was set as 0.45 in the experiments in order to expand its dynamic response range. The experimental results show a theoretical relationship in which normalized gray level is inversely proportional to the square of the distance. The theoretical results obtained by assuming the arc as a point source are in agreement with the experimental results in relative long distances, but not proper for relative short distances. On the other hand, the theoretical results that were obtained by assuming the arc as an extended source agree well with the experimental results in a wide range of distances between the arc and reflected area. The geometrical effect of arc shape plays a large role in the variation of intensity of the reflected arc light. The extended source, including the geometrical effect of the light source, should be considered in the examination of the arc light in relatively short distances. But the intensity variation of the reflected arc in long distances differed somewhat with the results of the extended source model on specular surfaces, such as mild steel, because the CCD camera has a limited dynamic response range. In Fig. 8, two theoretical results from each assumption show the same tendency because the surface reflectance model of SUS304 stainless steel is represented as a mirror.

From these experimental and theoretical results, it can be concluded that the welding arc can be assumed as a point light source for establishing the reflectance model of arc noise, especially with long distances between the arc and reflection surface. In actual welding with the vision sensor, however, the welding arc should be assumed to be an extended light source

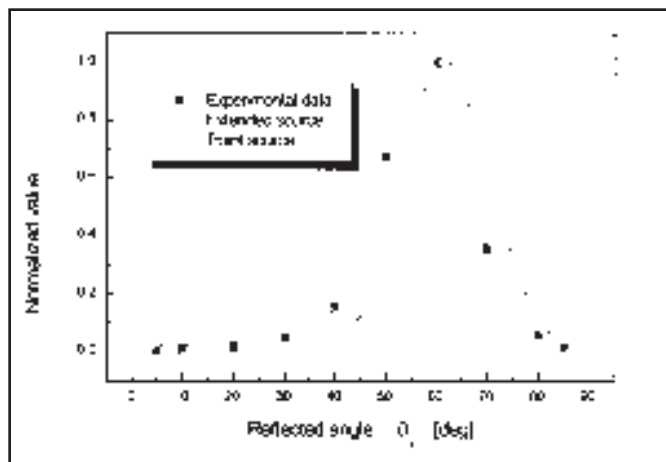


Fig. 11 — Intensity of gas tungsten arc reflected from mild steel with varying polar angle θ_r ($a = 30$ mm, $\theta_i = 60$ deg, $\phi_r = 0$ deg).

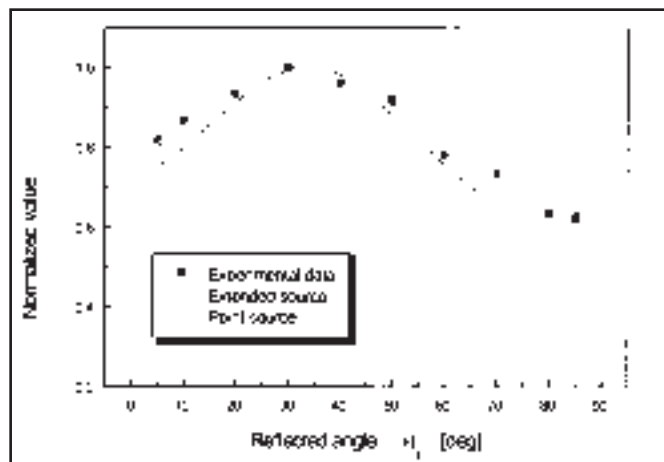


Fig. 12 — Intensity of gas tungsten arc reflected from Zn-coated container panel with varying polar angle θ_r ($a = 30$ mm, $\theta_i = 30$ deg, $\phi_r = 0$ deg).

because the arc is generally located a short distance from the viewing area of the vision sensor.

Figures 9 and 10 show the results of the experiment and the simulation for the arc in GTAW reflected from the hot-rolled mild steel surface and the Zn-coated container panel. The experiments were conducted for various azimuthal angles ϕ_r of reflection, while θ_p , θ_r , and a were fixed at 55 deg, 45 deg, and 30 mm, respectively. The specular characteristic was considerably higher around the same polar angle of reflection than around the incident polar angle; therefore, the experiments were carried out when each polar angle was different. This facilitated comparison of intensities corresponding to various azimuthal angles. By comparing the normalized data of the measured gray level with the simulated values, it was revealed that the extended source model with Torrance-Sparrow surface reflectance could adequately predict the reflectance behavior of the welding arc. The image pixel area was larger than the infinitesimal area of the theoretical model, which resulted in some difference between simulation and experiment. Thus, these results can be used effectively for designing visual joint tracking sensors for the arc welding process. Also, the influence of arc light in the vision sensor, which is at slightly tilting angle, can be decreased.

Figures 11 and 12 show the results of experiment and simulation for a GTAW arc reflected from a hot-rolled mild steel surface and a Zn-coated container panel. The experiments were carried out for various polar angles θ_r of reflection in the incident plane, while a was fixed at 30 mm. Peak values of the simulation results shifted somewhat more at the reflected angle than at the same angle of the incident beam; these results were caused by the characteristics of the geometrical attenuation factor in the surface reflectance model. But the peak gray levels of the reflected arc occurred around the polar angle of incident light, which could cause substantial noise in the image data. This effect appeared clearly with the reflection from mild steel, because its surface reflectance model largely represented the characteristics of the specular lobe and spike compared to the Zn-coated container panel. These phenomena were caused by their surface reflectance characteristics.

Conclusions

It was demonstrated that arc light should be assumed as an extended light source in the reflectance model for relatively short distances between the welding arc and base metal because the geometrical relationship of the arc shape has largely affected the re-

flected area in a relative short distance between the welding arc and the reflected area of the base metal.

In order to avoid the influence of the reflected arc light from the base metal, vision sensors must be designed using a little tilting angle and should be positioned as far out of the incident plane as possible. The proposed models and experimental results can be used effectively to design the configuration and moving path of vision sensors according to the base metal shape; they can thus reduce the effect of arc noise on vision sensors and consequently improve their reliability in automatic joint tracking in the arc welding process.

Acknowledgment

This work has been performed under the nuclear research and development program sponsored by the Ministry of Science and Technology, Korea.

References

1. Yu, J. Y., and Na, S. J. 1997. A study on vision sensors for automatic welding of height-varying weldment — Part I: Mathematical model. *Mechatronics* 7(7): 599–612.
2. Yu, J. Y., and Na, S. J. 1998. A study on vision sensors for automatic welding of height-varying weldment — Part II: Application. *Mechatronics* 8(1): 21–36.
3. Yu, J. Y., Na, S. J., Kang, G. H., and Han, Y. S. 1995. Development of an automatic welding system for corrugated membranes of the LNG tank. *Proceedings of the International Conference on the Joining of Materials (JOM-7)*, Helsinki, Denmark, pp. 519–525.
4. Shaw, C. B., Jr. 1975. Diagnostic studies of the GTAW arc: Part 1 — Observational studies. *Welding Journal* 54(2): 33-s to 44-s.
5. Shaw, C. B., Jr. 1975. Diagnostic studies of the GTAW arc: Part 2 — Mathematical model. *Welding Journal* 54(2): 81-s to 84-s.
6. Kim, E. W., Allemand, C., and Eagar, T. W. 1987. Visible light emissions during GTAW and its application to weld image improvement. *Welding Journal* 66(12): 369-s to 377-s.
7. Sliney, D. H., Moss, C. E., Miller, C. G., and Stephens, J. B. 1982. Transparent welding curtains. *Welding Journal* 61(3): 17-s to 24-s.
8. Yuuki, M., and Tejima, A. 1988. Development of visual welding sensors and feedback control of molten pool. *IHI Engineering Review* 21(3): 94–98.
9. Brzakovic, D., and Khani, D. T. 1991. Weld pool edge detection for automated control of welding. *IEEE Trans. on Robotics and Automation* 7(3): 397–403.
10. Voelkel, D. D., and Mazumder, J. 1990. A visualization of a laser melt pool. *Applied Optics* 29(12): 1718–1720.
11. Gorgon, S. S., Flanigan, L. A., and Dyer, G. E. 1987. Development of a CCTV system for welder training and monitoring of space shuttle main engine welds. *Welding Journal* 66(3): 47-s to 54-s.
12. Yen, L., Lin, W., and Dinghua, C. 1986. A study on direct vision sensor for welding visual sensing. *Proceedings of the 6th International Conference on Robot Vision and Sensory Controls*, Paris, France, pp. 245–248.
13. Cullison, A., and Irving, B. 1992. Where in the world is the weld? *Welding Journal* 71(8): 45–49.
14. Yoo, W. S., Yu, J. Y., and Na, S. J. 1999. Application of vision sensor for welding automation. *2nd Joint Korea-Australia Workshop on Manufacturing Technology on Steel Processing*, Postech, Pohang, Korea, pp. 42–46.
15. Yu, J. Y., Na, S. J., Kang, G. H., and Han, Y. S. 1996. A study on development of automatic welding system for corrugated membranes of the LNG tank. *Journal of KWS* 14(1): 62–69.
16. Nenef, L., and Gardner, C. S. 1985. Optical emissions from weld arcs and their effects on the performance of welding robot vision systems. *Applied Optics* 24(16): 2587–2595.
17. Nakata, S., Jie, H., Tsuruha, Y., Noguchi, N., and Kobashiri, T. 1989. Determination on geometrical arrangement of optical equipment and photographic parameters for construction of visual sensing system. *Quarterly Journal of the Japan Welding Society* 17(3): 358–362.
18. Lambert, J. H. 1760. *Photometria, sive de mensura et gradibus luminis, colorum et umbrae*, Augsburg, Germany, Eberhard Klett.
19. Torrance, K. E., and Sparrow, E. M. 1966. Off-specular peaks in the directional distribution of reflected thermal. *Journal of Heat Transfer-Trans. of ASME(C)* 88(2): 223–230.
20. Nayar, S. K., Ikeuchi, K., and Kanade, T. 1991. Surface reflection: physical and geometrical perspectives. *IEEE Trans. Pattern Analysis and Machine Intelligence* 13(7): 611–634.
21. Inoue, K. 1981. Image processing for on-line detection of welding process (Rep. 3) — improvement of image quality by incorporation of spectrum of arc. *Trans. of Japan Welding Research Institute* 10(1): 13–18.
22. Lee, C. W., and Na, S. J. 1996. A study on the influence of reflected arc light on vision sensors for welding automation. *Welding Journal* 75(12): 379-s to 387-s.
23. Wang, Q. L., and Li, P. J. 1997. Arc light sensing of droplet transfer and its analysis in pulsed GMAW process. *Welding Journal* 76(11): 458-s to 469-s.
24. Li, P. J., and Zhang, Y. M., 2000. Analysis of arc light mechanism and its application in sensing of GTAW process. *Welding Journal* 79(9): 252-s to 260-s.
25. Lee, S. Y., and Na, S. J., 1996. A numerical analysis of stationary TIG welding arc considering various electrode angles. *Welding Journal* 75(9): 269-s to 279-s.
26. Torrance, K. E., and Sparrow, E. M. 1967. Theory for off-specular reflection from roughened surface. *Journal of the Optical Society of America* 57(9): 1105–1114.